Impact of future land cover changes on HNO_3 and O_3 surface dry deposition.

T. Verbeke[1], J. Lathière[1], S. Szopa[1], N. de Noblet-Ducoudré[1]

[1] {Laboratoire des Sciences du Climat et de l'Environnement - LSCE-IPSL, CEA/CNRS/UVSQ, Gif-sur-Yvette, France}

Correspondence to: J. Lathière (juliette.lathiere@lsce.ipsl.fr)

Abstract

Dry deposition is a key component of surface-atmosphere exchange of compounds, acting as a sink for several chemical species. Meteorological factors, chemical properties of the trace gas considered and land surface properties are strong drivers of dry deposition efficiency and variability. Under both climatic and anthropogenic pressure, the vegetation distribution over the Earth has been changing a lot over the past centuries, and could be significantly altered in the future. In this study, we perform a modeling investigation of the potential impact of land-cover changes between present-day (2006) and the future (2050) on dry deposition velocities at the surface, with special interest for ozone (O_3) and nitric acid (HNO_3), two compounds which are characterized by very different physico-chemical properties. The 3D chemistry transport model LMDz-INCA is used, considering changes in vegetation distribution based on the three future projections RCPs 2.6, 4.5 and 8.5, and present-day (2007) meteorology. The 2050 RCP 8.5 vegetation distribution leads to a rise by up to 7% (+0.02 cm/s) in the surface deposition velocity calculated for ozone (V_{d,O_3}) and a decrease of -0.06 cm/s in the surface deposition velocity calculated for nitric acid (V_{d,HNO_3}) relative to the present day values in tropical Africa, and up to +18% and -15% respectively in Australia. When taking into account the RCP 4.5 scenario, which shows dramatic land cover change in Eurasia, V_{d,HNO_3} increases by up to 20% (annual-mean value) and reduces V_{d,O_3} by the same magnitude in this region. When analyzing the impact of

surface dry deposition change on atmospheric chemical composition, our model calculates that the effect is lower than 1 ppb on annual mean surface ozone concentration, for both the RCP8.5 and RCP2.6 scenarios. The impact on HNO_3 surface concentrations is more disparate between the two scenarios, regarding the spatial repartition of effects. In the case of the RCP 4.5 scenario, a significant increase of the surface O_3 concentration reaching locally by up to 5 ppb (+5%) is calculated on average during the June-August period. This scenario induces also an increase of HNO_3 deposited flux exceeding locally 10% for monthly values. Comparing the impact of land-cover change to the impact of climate change, considering a 0.93°C increase of global temperature, on dry deposition velocities, we estimate that the strongest increase over lands occurs in the North Hemisphere during winter especially in Eurasia, by +50% (+0.07 cm/s) for V_{d,O_3} and +100% (+0.9 cm/s) for V_{d,HNO_3}. However, different regions are affected by both changes, with climate change impact on deposition characterized by a latitudinal gradient, while the land-cover change impact is much more heterogeneous depending on vegetation distribution modification described in the future RCP scenarios. The impact of long-term land-cover changes on dry deposition is shown to be significant and to differ strongly from one scenario to another. It should therefore be considered in biosphere-atmospheric chemistry interaction studies in order to have a fully consistent picture.

1. Introduction

Amongst surface-atmosphere interactions, dry deposition plays a key role in the exchange of compounds and acts as a significant sink for several atmospheric species. Performing an intercomparison of 26 state-of-the-art atmospheric chemistry models, Stevenson et al. (2006) estimated the surface removal of ozone by dry deposition to be about 1000±200 Tg/yr on average, with values ranging from 720 to 1507 Tg/yr amongst models, compared to 5100, 4650 and 550 Tg/yr for chemical production, chemical destruction and stratospheric input fluxes respectively. This study also underlined that although global deposition fluxes are consistent between models, locally, there is a large variability in the ozone deposition velocities (Stevenson et al., 2006). Since all these models use deposition schemes based on Wesely's prescription (Wesely et al., 1989), the discrepancies suggest different hypotheses for the land-type consideration. Based on satellite measurements from OMI (Ozone Monitoring Instrument) combined with the Goddard Earth Observing System chemical transport model (GEOS-Chem),

Nowlan et al. 2014 estimated dry deposition to land to be 98% of total deposition for NO_2 and 33% for SO_2. This deposition fluxes over land represent 3% of global NOx emissions and 14% of global sulfur emissions. Land surfaces can therefore play a significant role on deposition, with a highly variable contribution from one chemical compound to another.

The air-surface exchange of trace compounds has been shown to be strongly variable, especially between different types of surface vegetation and soil characteristics (Wesely et al., 2000). Regarding ozone, model data differences reported in the literature could be attributed to oversimplifications in the implementation of the dry deposition scheme (Val Martin et al. 2014) since many models rely on "resistance in series" schemes developed in the 1980s (Hardacre et al. 2005).

In order to quantify the non-photochemical sink for tropospheric burden at the regional and global scales, the scientific community uses numerical dry deposition schemes calibrated with field-measurements of dry deposition velocities (Wesely et al., 1989, Zhang et al., 2002b), implemented usually in chemistry-transport models. Dry deposition efficiency is influenced by multiple meteorological factors (temperature, solar radiation, humidity and especially atmospheric turbulence), chemical properties of the trace gas considered (solubility, oxidative capacity), and land surface properties (surface type, surface roughness, foliar surface and ecosystem height in the case of vegetation surfaces). Some of these factors are poorly constrained and are thus accounted for in deposition schemes in a very simplistic way. The vegetation distribution for instance is usually prescribed using maps for the region of interest that are generally kept the same for either past, present or future studies (e.g. Andersson and Engardt, 2010 or Lamarque et al. 2013). There is therefore a lack of knowledge regarding the impact of long-term changes in vegetation distribution on dry deposition chemical compounds at the surface. Since the beginning of the industrial era, human activities have modified the use of large surfaces, affecting significantly the vegetation distribution, especially in the northern temperate latitude regions. Further land cover modifications are expected in the 21st century, due to projected increases in energy and food demands, and vegetation, in tropical regions in particular, could undergo drastic alterations.

Only a few studies have been carried out recently on the dry deposition changes in the future. Some of them focus on the impact of climate change on the dry deposition (Andersson and Engardt, 2010) while others combine the effects of several future changes (climate, CO_2 levels,

land cover) on atmospheric chemistry in general (Ganzeveld et al. 2010, Wu et al. 2012). However, considering anthropogenic land cover changes among other large modifications of the vegetation/atmospheric chemistry drivers does not allow to identify if the land cover change should be or not considered as a priority in the studies of future atmospheric chemistry. The objective of this study is to investigate and isolate the potential impact of land-cover changes between the present-day (2006) and the future (2050) on dry deposition velocities at the surface, using a modeling approach with a 3D chemistry transport model as illustrated in Figure 1. Changes in vegetation distribution are based on the three future projections known as Representative Concentration Pathways scenarios (RCPs) (van Vuuren et al. 2011), developed for the climate model intercomparison project (CMIP5): RCPs 2.6, 4.5 and 8.5. For this work we focus on ozone (O_3) and nitric acid (HNO_3), two compounds which are characterized by very different biophysical properties (e.g. solubility and oxidative capacity). In section 2, we describe the chemistry-transport model LMDz-INCA, the dry deposition module and the modeling strategy adopted. In section 3, we describe the different future land cover changes as given in the three RCP scenarios 2.6, 4.5 and 8.5, and explain their impacts on surface dry deposition velocities of ozone and nitric acid. Finally, the magnitude of land cover effects related to climate change on dry deposition velocities by 2050 is discussed.

2. Modeling set up

In our study, the global chemistry-climate model LMDz-INCA (Hauglustaine et al., 2004) is used to compute dry deposition. LMDz (v4) is an atmospheric general circulation model that simulates the transport of trace species. The model is run with 19 hybrid levels from the surface to 3hPa at a horizontal resolution of 1.85° in latitude and 3.75° in longitude. It is coupled on-line to the chemistry and aerosols model INCA (v2) which computes concentrations of reactive tracers considering their emissions, chemical transformations, transport and deposition processes. The atmospheric oxidation reactions of CH_4, CO and non-methane hydrocarbons are documented in Folberth et al. (2006). In order to be able to isolate the effect of land-cover change only on the atmospheric chemical composition, through change in surface dry deposition, emissions are prescribed according to Lamarque et al. (2010) for anthropogenic fluxes and Lathière et al. (2006) for biogenic VOCs, as described in Szopa et al. (2013), and are kept constant between all runs.

2.1 Dry deposition in LMDz-INCA

The chemical deposition scheme used in INCA is based on the parameterization of Wesely (1989) and Wesely and Hicks (2000), computing dry deposition velocity V_d as a succession of resistances as follows:

$$|V_d(z)|=[R_a(z)+R_b+R_c]^{-1}$$

where R_a is the aerodynamic resistance, R_b the quasi-laminar resistance, and R_c the bulk surface resistance.

R_a determines the ability of the airflow to bring gases or particles close to the surface, and depends mainly on the atmospheric turbulence structure and on the height considered. In this paper, we will focus on dry deposition at the surface, ground level (z=0). R_b describes the resistance to the transfer very close to the surface and is driven by the surface (surface roughness) and the gas or particle (molecular diffusivity) characteristics. R_a and R_b are calculated based on Walcek et al. (1986). The surface resistance R_c represents the different pathways through which the gas or particles can deposit and is determined by the affinity of the surface for the chemical compound. Deposition can thus occurs directly on the ground and/or, in the case of vegetative surfaces, on the different vertical layers of the canopy on trunks, branches and mainly on leaves, through stomata or cuticles (Wesely, 1989). Vegetation surfaces in particular cover a large area of the Earth, with a high spatial and seasonal variability due to species diversity. Environmental conditions such as atmospheric CO_2 or pollutant (ozone) concentrations, radiation, temperature, or the occurrence of possible stress (drought for instance) can strongly affect the vegetation functioning, and the stomatal opening especially, and therefore impact dry deposition velocity. The impact of vegetation type, distribution and functioning, on dry deposition is still not well understood and generally very simply, if at all, considered in chemistry-transport models (Hardacre et al., 2015). For all chemical species considered in LMDz-INCA, R_c is based on their temperature dependent Henry's Law effective coefficient and reactivity factor for the oxidation of biological substances (Folberth et al., 2006). The coefficients for Henry's Law are taken from Sander (1999) and reactivity factors are taken from Wesely (1989) and Walmsley and Wesely (1996).

The dry deposition scheme implemented in LMDz-INCA considers eleven surface categories: (1) urban land, (2) agricultural land, (3) range land, (4) deciduous forest, (5) coniferous forest, (6)

mixed forest including wetland, (7) water, both salt and fresh, (8) barren land, mostly desert, (9) non-forested wetland, (10) mixed agricultural and range land, and (11) rock open areas with low-growing shrubs. This scheme was originally developed by Wesely (1989) and updated by Wesely and Hicks (2000) for Northern hemisphere regions of United States and southern Canada regions. Five seasonal categories are used as proxy of vegetation growth stage (midsummer with lush vegetation; autumn with unharvested cropland; late autumn after frost, no snow; winter, snow on ground, and subfreezing; transitional spring with partially green short annuals). For global scale study purposes, the scheme in LMDz-INCA has been modified in order to represent the different seasonal cycles throughout the world. The latitude dependency of the vegetation seasonality is described by dividing the globe into three belts: Northern hemisphere regions (latitude > 33°N); Tropical regions (33°S < latitude < 33°N) and Southern hemisphere regions (latitude < 33°S). Summer is considered in the tropics throughout the whole year, describing the evergreen vegetation. Two opposite seasonal cycles are taken into account in extra-tropical Northern and Southern hemisphere regions, with winter being activated when snow falls. The deposition of atmospheric compounds on plant leaves, through stomata especially, is determined following the Wesely (1989) approach. The stomatal resistance depends on vegetation type, seasonal category, radiation and temperature, but the potential impact of other environmental conditions such as drought, or atmospheric concentration of CO_2 or ozone, are not considered. The dry deposition velocity over each grid box is eventually determined by summing deposition velocities computed over every land cover types, weighted by their respective fractional surface coverage (ranging from 0 to 1).

The deposition velocities computed by LMDz-INCA based on a different land cover distribution was evaluated in Hauglustaine et al. (2004). This work illustrates values generally consistent with typical deposition velocities highlighted for North America and Europe as presented in Wesely and Hicks (2000) and monthly values reaching up to 0.6 cm/s for ozone and up to 3 cm/s for HNO_3 over land. In the supplementary material the ozone dry deposited fluxes simulated by LMDz-INCA in the present-day simulation and used in this study are compared to other global model and long term measurements which are discussed in Hardacre et al. (2015).

2.2 Land use and land cover changes between 2007 and 2050

The present-day distribution of vegetation categories considered in LMDz-INCA is illustrated in Figure 2 as dominant type, covering the largest fraction of each gridbox. Crops are dominant mainly in restricted temperate regions of North America, Central Europe, and also in India, while range lands are largely spread. Deciduous forests dominate in tropical regions of South America, Africa and Indonesia, together with Central and Southern Europe, while coniferous forests have a high occupancy in boreal regions of North America and Eurasia. Figure 2 also shows the 10 regions of special interest selected for this study, which will be considered in more detail when analyzing our results.

Future maps are based on scenarios of land-cover changes derived from four different Representative Concentration Pathways (RCPs; Moss et al. 2010; van Vuuren et al. 2011) and four Integrated Assessment Models (one per RCP) (RCP 8.5, RCP 4.5 and RCP 2.6). Those maps were further harmonized to ensure smooth transitions with past/historical changes (Hurtt et al. 2011). Those datasets only provide information on human activities (crop land and grazed pastureland) in each grid-cell (at a 0.5° resolution) but do not provide any recommendation regarding the distribution of natural vegetation. We have therefore combined them with our original present-day land-cover map (Loveland et al. 2000), which already includes both natural and anthropogenic vegetation types, following a methodology described in Dufresne et al. (2013). Figure 3 illustrates changes in vegetation fraction for agriculture and grasslands on one hand, and for forests on the other hand, between present-day (distribution for 2007) and the future RCP scenarios. For most affected regions, the changes in land surfaces are presented in Figure 4. The RCP 4.5 scenario shows the largest surface change with a total of 20.8 x 10^6 km², representing 10.4% of the 70°S-70°N Earth continental surface. According to the RCP 2.6 and RCP 8.5 scenarios only 15 to 16.8 x 10^6 km² of land cover surfaces are converted.

The RCP 2.6 scenario is characterized by a moderate increase of energy consumption throughout the 21st century together with a decrease in oil consumption. The energy supply is thus partly ensured by bioenergy production increase (van Vuuren et al, 2011). Such hypotheses lead to a strong expansion of agricultural lands (+ 2.61 x 10^6 km² globally) at the expense of forests (- 1.40 x 10^6 km²) and grasslands (- 1.15 x 10^6 km²) targeting mainly Eurasia, US and tropical southern America.

The RCP 8.5 scenario, characterized by the strongest increase in population and energy consumption, amongst RCPs), assumes a large increase in global population until 2050. The

resulting demand for food leads to a strong expansion of land used for crops and pastures at the expense of forests. The tropical belt (from 30°N to 30°S) undergoes the largest changes: tropical forests in southern America and southern Africa are partially harvested (1.0×10^6 km² totally, i.e. 13% of their 2007 extent) and replaced by grassland and crops, while in Eastern Australia, forests lose 7% ($- 0.28 \times 10^6$ km²) of their 2007 area and are replaced by grasslands which gains 0.12×10^6 km² on desert.

The "mitigation" RCP 4.5 scenario is a rather contrasting scenario as it proposes a strong increase in the cover of all forest categories, a small expansion of grasslands but an important recession of agricultural surfaces mainly in developed countries. Indeed Eurasia, US and Canada undergo a strong conversion from agriculture and grassland to forests with a magnitude change of $\sim 0.8 \times 10^6$ km² in Eurasia and $\sim 0.4 \times 10^6$ km² in northern US and Canada. Besides, tropical southern America loses 0.55×10^6 km² of cumulated croplands and grasslands but forests expand by the same surface between present day and 2050.

Finally, it is important to underline that the 3 RCP scenarios offer a wide variety of land cover change projections. They all are quite different compared to previous scenarios, such as the SRES-A2 investigated by Ganzeveld et al. (2010), characterized by a strong North/South contrast, with the tropical and southern hemisphere countries mainly encountering deforestation whereas northern areas (>35°N) were mainly projected to see afforestation.

2.3 Simulation strategy

In order to quantify the effects of these land cover changes on surface dry deposition, we carried out two sets of simulations (Table 1). The first set intends to isolate the effect of future possible land cover changes on dry deposition without any climate change. It includes one control run (present day), using 2006 vegetation distribution (Figure 2) and three future runs using the 2050 vegetation maps according to the RCPs 8.5, 4.5 and 2.6 scenarios. The same present-day meteorology, biogenic and anthropogenic emissions are used in these four simulations. These simulations are run for 1 year with wind and temperature fields being relaxed towards the ECMWF ERA-interim reanalysis (Dee et al., 2011) with a time constant of 6 hours.

Then a second set of two simulations is performed in order to investigate the effect of future climate change on deposition and compare it with the impact of future land cover change: one run for the 2000-2010 period and a second run for the 2045-2055 period. Those simulations are

243 performed without nudging and the LMDz general circulation model requires sea surface
244 temperature (SST), solar constant and Long-Lived Green House Gases (LL-GHG) global mean
245 concentrations as forcings. For historical simulations, we use the HADiSST for sea surface
246 temperature (Rayner et al., 2003) and the evolution of LL-GHG concentrations compiled in the
247 AR4-IPCC report. For future projections, we use the SST from IPSL-CM4 simulation for the
248 SRES-A2 scenario, which induce similar climate trajectories in terms of radiative forcing than
249 RCP8.5. We use the LL-GHG concentrations distributed by the RCP database for RCP8.5
250 projection for the 2045-2055 period. Eleven years are run and averaged to allow smoothing of
251 interannual climate variability. The mean surface temperature change is 0.93°C between future
252 simulation and present day simulation. Both experiments use the same present-day vegetation
253 distribution, anthropogenic and biogenic emissions.
254
255 ## 3. Results
256 ### 3.1. Present day ozone and nitric acid deposition
257 First of all, we present the deposition over continental regions for present-day conditions (Figure
258 5) by illustrating the annual means of deposition velocities at the surface, surface concentrations
259 and deposited fluxes for O_3 and HNO_3.
260 The highest ozone deposition velocities (>0.35 cm/s) are simulated over India, south-eastern
261 Asia, western coast and center of South America, Mexico, Europe and sub Saharan Africa and
262 Australia. Hence, those areas are mainly covered by crops and grasses, where the highest V_{d,O_3}
263 occurs, while Europe and Southeast Asia are mainly covered by deciduous forests, with therefore
264 lower annual V_{d,O_3}. O_3 surface dry deposition is indeed maximal over small canopies vegetation
265 and minimal over bare soil with deposition affinity ranging from Agriculture > Grasslands >
266 Deciduous > Coniferous > Bare soil (see sensitivity tests in supplementary material).
267 Temperate regions see ozone deposition velocities significantly reduced in winter (see
268 supplementary material for seasonal means) whereas tropical regions, covered mainly by small
269 canopies, are characterized by surface deposition velocity exceeding 0.35 cm/s throughout the
270 whole year due to the lack of seasonality in the vegetation phenology in the global model. In
271 temperate regions of the Northern hemisphere, the highest deposition velocities for ozone reach
272 values of 0.4 cm/s to 0.6 cm/s for V_{d,O_3} over Europe.

For HNO_3, the annual mean deposition velocities are maximum over Brazil, Western Europe, India, Indochinese Peninsula and South of western Africa (> 1.6 cm/s in annual mean). V_{d,HNO_3} reaches maximum values over deciduous and coniferous forests, due to deposition affinity ranking from: Deciduous, Coniferous > Agriculture > Grasslands > Bare soil. This is due to the strong dependency of V_{d,HNO_3} to surface roughness (Walcek et al., 1986). For temperate region and South Asia, the HNO_3 deposition is strongly affected by the vegetation cycle with maximum in July between 2.5 cm/s and 3.5 cm/s. This is remarkable over temperate and boreal forests. In the tropics, Amazonian forest encounters high HNO_3 deposition velocity in winter whereas deposition velocity over African equatorial forest is limited throughout the whole year. (see supplementary material for seasonal means of deposition). Large areas receive high HNO_3 deposition fluxes exceeding 0.5g(N)/m^2/yr in annual mean: North eastern USA, western Europe and East Asia. These areas correspond to the ones identified by Dentener et al. 2006 and in which natural vegetation encounters nitrogen deposition higher than the "critical load" threshold of 1g(N)/m^2/yr.

The repartition of deposited fluxes is strongly affected by the large variability of atmospheric concentrations of ozone and nitric acid in the surface layer. For both O_3 and HNO_3, the deposited fluxes are maximum over South and East Asia and eastern North America and central and Western Europe. For ozone, the maximum in winter is over central Africa whereas in summer the ozone deposition is maximum over central Europe and eastern US. For HNO_3, the deposited flux repartition is equally driven by the deposition velocity and by the HNO_3 surface concentration distribution. In winter, HNO_3 is maximally deposited over eastern US, central Africa, central Europe India and East Asia. In summer, regions are the same in the Northern hemisphere but the extension of deposited HNO_3 areas is higher and the deposition in Africa is weak, due to weak HNO_3 concentration.

3.2. Impact of 2050-2007 land cover changes on surface dry deposition velocities.

We then analyze the changes in surface dry deposition velocities between present day and 2050 induced only by land cover change. Four regions undergo interesting land cover changes in terms of intensity or contrast between scenarios: Eurasia, North America, tropical Africa and Australia. The left columns of Figures 6 and 7 show the relative difference in surface dry deposition velocities distribution for O_3 and HNO_3, resulting from the changes in vegetation distribution

between 2007 and 2050 for the 3 RCP scenarios. We shall first describe the two scenarios projecting weak land cover changes for 2050s: RCP8.5 and RCP2.6. In the RCP 8.5 scenario, one main land cover change is the expansion of agricultural land at the expenses of forests. According to this scenario, over tropical Africa, the maximal land cover change occurs locally with fraction of deciduous forests decreasing by up to 0.2 while cropland fraction increases by up to 0.2 in the same region. This induces a rise by up to 7% (+0.02 cm/s) in V_{d,O_3} and a decrease of 0.06 cm/s in V_{d,HNO_3} relative to the present day values in this area. These order of magnitude and sign of changes are consistent with sensitivity tests in which we replaced totally forests by croplands inducing an increase of 0.1 cm/s in V_{d,O_3} and a decrease of 0.5 cm/s in V_{d,HNO_3} (during summer and winter). The strongest LCC occurs in Australia (-0.12 in forest fraction and +0.2 in grassland fraction in eastern Australian regions), which induces a local maximum increase of 18% (+0.05 cm/s) in V_{d,O_3} and a maximum decrease of 15% in V_{d,HNO_3} (-0.1 cm/s). We find the same order of magnitude in changes induced by land cover change in Western Australia but with a different sign for V_{d,HNO_3} changes (+0.1cm/s ; +9%), due to a different type of shift in surface covering (+0.12 in grassland fraction, -0.10 for desert).

As land cover changes are weak in the RCP 2.6 scenario, a more dispersed and weaker effect on surface dry deposition velocities is simulated (maximum absolute difference of 10%).

According to the RCP 4.5 scenario, the most dramatic land cover change occurs in Eurasia where local maximum changes by up to 0.5 in fraction of vegetation are projected, involving in most cases an increase in forest surfaces at the expense of agricultural areas. This increases V_{d,HNO_3} by up to 20% (annual-mean value) and reduces V_{d,O_3} by the same magnitude in this region. The LCC impacts are stronger by a factor 4 to 6 in summer both on O_3 and HNO_3 deposition velocities. This difference in deposition velocities between winter and summer were highlighted in sensitivity tests which see a strong decrease in V_{d,O_3} during the June-August period (up to 0.15 cm/s in absolute) and a strong increase in V_{d,HNO_3} (up to 1.5 cm/s) underlining a total conversion of croplands to forests. This is due to a higher surface roughness which enhances the deposition velocity of HNO_3 (via the reduction of the aerodynamic resistance). However, the higher input surface resistance (prescribed in the model and variable relating to season indexes) reduces V_{d,O_3} even combined to a warmer climate which decreases the stomatal resistance (Rs).

3.3. Impact on atmospheric composition

The objective of this part is to isolate the effects of dry deposition changes due to land cover changes on the tropospheric concentration of O_3 and HNO_3. Therefore, solely the impact of land cover changes on deposition at the surface is considered between the present-day and 2050 simulations. This impact on surface concentrations of O_3 and HNO_3 is shown in the right columns of Figures 6 and 7.

For both the RCP8.5 and RCP2.6 scenarios, the LCC effects through deposition are lower than 1 ppb on annual mean surface ozone concentrations. In term of relative difference, only the reduction of ozone over Australia when considering RCP8.5 hypotheses is exceeding 1%, reaching up to 5% at some points. The impact on HNO_3 surface concentrations is more disparate between the two scenarios when considering the spatial repartition of effects. The RCP8.5 scenario leads to local increase of HNO_3 due to the reduction in the deposition velocity. This HNO_3 increase is notable over Mexico, Brazil, western and South Africa (comprised in the 1-6% interval). Land cover change in Australia leads to an increase exceeding 7% in the east and a decrease reaching 5% in the west.

The RCP4.5 scenario induces the strongest impacts on deposition velocity with a reduction of V_{d,O_3} (-0.08 cm/s) occurring in Eurasia due a strong reduction in croplands occupancy (-0.6 in fraction of coverage) and a strong increase in forest distribution (+0.6 in fraction of coverage) between 2007 and 2050. It induces a significant increase of the surface O_3 concentration reaching locally by up to 5 ppb (+5%) on average during the June-August period. This scenario induces also an increase of the HNO_3 deposition flux exceeding locally 10% for monthly values. In Eurasia and eastern North America. It thus leads to a reduction in the HNO_3 concentration by 0.2 ppbv in Eurasia (-13%) and in North America (-8%), mainly due to changes in nitric acid velocities of +0.5 cm/s and +0.2 cm/s respectively.

3.4 Are the land cover induced changes significant compared with the climate change impact?

The impact of land-use changes on deposition can be compared to the one of climate in order to discuss their respective strength on deposition velocities. To this purpose, we consider a 0.93°C increase of global temperature, corresponding to the temperature increase projected in the RCP scenarios between the beginning and the middle of the 21st century. The figure 8 shows the

impact of this climate change on the deposition velocity for O_3 and HNO_3. We see that the strongest increase in surface dry deposition velocities over lands occurs in the North Hemisphere during winter especially in Eurasia (+50% (+0.07 cm/s) for V_{d,O_3} and +100% (+0.9 cm/s) for V_{d,HNO_3}). The climate effect on the deposition velocity by affecting stomatal resistance, sensitive to surface temperature and solar irradiance, can locally reach values far more important than the LCC. The Table 2 presents the effects of land cover change considering RCP4.5 projection and climate change on deposition velocity averaged over 10 regions for O_3 and HNO_3. In several regions, the effect of land cover change is of the same order of magnitude than the one of climate. The modification in land cover affectation can thus amplify the climate change effect or, when the sign is the opposite, counterbalances it.

4. Discussion and conclusions

Using the 2.6, 4.5 and 8.6 RCP scenarios for land-use change between 2000s and 2050s, simulations were carried out with the global chemistry-transport model LMDz-INCA in order to assess the impact of changes in vegetation distribution on the dry deposition of ozone and nitric acid at the surface and on atmospheric composition.

Regarding vegetation distribution, the largest change at the global scale is given in the RCP 4.5 scenario (20.8×10^6 km²), with surface converted being 28% and 19% lower in the RCP 2.6 and RCP 8.5 scenarios respectively. Projections show major changes in the Northern Hemisphere in the case of RCP 4.5 scenario, while Australia and Africa are mostly affected in the RCP 8.5 scenario.

Vegetation type and surface being key drivers of surface dry deposition, any change in vegetation distribution can potentially affect dry deposition velocity and therefore atmospheric chemical composition. Considering the 2050 RCP 8.5 vegetation distribution leads to a rise by up to 7% (+0.02 cm/s) in V_{d,O_3} and a decrease of 0.06 cm/s in V_{d,HNO_3} relative to the present day values in tropical Africa, and up to +18% and -15% respectively in Australia. As land cover changes are weak in the RCP 2.6 scenario, a more dispersed and weaker effect on surface dry deposition velocities is simulated (maximum absolute difference of 10%) when considering the RCP 2.6 scenario, characterized by a moderate change in vegetation distribution compared to present-day. When taking into account the RCP 4.5 scenario, which shows dramatic land cover change in Eurasia, V_{d,HNO_3} increases by up to 20% (annual-mean value) and reduces V_{d,O_3} by the same

magnitude in this region. When analyzing the impact of dry deposition change on atmospheric chemical composition, our model calculates that the effect is lower than 1 ppb at the grid box scale on annual mean surface ozone concentration, for both of the RCP8.5 and RCP2.6 scenarios. The impact on HNO_3 surface concentrations is more disparate between the two scenarios, regarding the spatial repartition of effects. In the case of the RCP 4.5 scenario, a significant increase of the surface O_3 concentration reaching locally up to 5 ppb (+5%) is calculated on average during the June-August period. This scenario induces also an increase of HNO_3 deposited flux exceeding locally 10% for monthly values. Investigating the impact of climate change, considering a 0.93°C increase of global temperature, on surface dry deposition velocities, we calculate that the strongest increase over lands occurs in the North Hemisphere during winter especially in Eurasia (+50% (+0.07 cm/s) for V_{d,O_3} and +100% (+0.9 cm/s) for V_{d,HNO_3}). The climate change impact on deposition is characterized by a latitudinal gradient, while the effect of land-cover change is much more heterogeneous. Both climate and vegetation distribution changes are of similar amplitude but sign can differ.

The objective in this study is to isolate the impact of land-cover change on atmospheric chemical composition through modification of surface dry deposition only rather than to consider comprehensively all the atmospheric chemistry/vegetation interactions affected by land cover change. Indeed, as far as long term evolution of atmospheric chemistry is investigated (e.g. Stevenson et al. 2006, Lamarque et al. 2010), the evolution of biogenic emissions due to global changes is discussed, if not shared between models, but the land cover maps used for dry deposition remain unchanged. Here we want to assess the importance of this choice. Land cover changes would go together with changes in surface emissions, either from anthropogenic, agricultural, or biogenic sources, with changes in climate, and possible strong consequences on the atmospheric chemical mechanism and surface-atmosphere interactions. In an attempt to quantify all the effects of land cover change, those processes would therefore need to be considered altogether to get a better picture of the overall resulting effect. However they all have large uncertainties and added to error compensation effects, the dry deposition change can be can masked by other process changed (see for example Wu et al., 2012). Moreover, the sensitivity of biogenic emissions to climate and CO_2 changes as well as the level of coupling between vegetation and chemistry are so different from one model to another that the full land cover change response is for the moment highly model-dependent.

Fowler et al. (2009) underline an uncertainty of about 50% in the ability of models to estimate dry deposition fluxes for main chemical species, the lack of measurements making a proper and extensive model evaluation especially difficult. Hardacre et al. (2015), who compared the dry deposition of ozone of 15 global atmospheric chemistry-transport models with measurements in Europe and North America underline discrepancies of up to a factor of two, notably in the summer maximum, but do not find a systematic model bias. Dry deposition in global models is still largely based on the in-series resistance approach proposed by Wesely (1989) and generally do not integrate more recent findings demonstrated by field or laboratory studies (Hardacre et al., 2015).

Vegetation is usually crudely described in chemistry-transport models, with leaf surface or cuticle and stomatal resistances for instance being prescribed or very simply parameterized, and lack of the representation of seasonal variation or stress (water, temperature) impacts. This could lead to significant uncertainty in model representation and projections of atmospheric chemical composition and surface-atmosphere interactions. The work by Wesely and Hicks (2000) underlines that selecting proper input parameters for dry deposition schemes, such as stomatal, cuticle, and soil resistances, is crucial for a satisfactory determination of dry deposition efficiency, for both simple and multi-layers models. Zhang et al. (2003) propose a revised parameterization of dry deposition including the leaf area index in the calculation of aerodynamic and cuticular resistances, which could give the possibility of a better representation of the impact of vegetation seasonality in dry deposition estimates. The roles of surface wetness, soil moisture, the partition between stomatal and non-stomatal uptake for instance, shown of high importance for dry deposition processes, are usually not implemented or poorly described in global models (Fowler et al., 2009; Hardacre et al., 2015). This is also the case of the LMDz-INCA model in which dry deposition is described through a highly parameterized approach. Investigating ozone non-stomatal uptake using measurements over five different vegetation types, Zhang et al. (2002a) show that the O_3 uptake by cuticles is affected by friction velocity, relative humidity, canopy wetness and LAI especially, and tends to increase with wetness and high humidity. A new parameterization for non-stomatal uptake is proposed and is expected to improve this deposition path in existing models, where a constant value is often considered, and could therefore be tested more largely in global models. Investigating the impact of coupling dry deposition to vegetation phenology in the Community Earth System Model (CESM) on ozone surface simulation, Val

Martin et al. (2014) show the importance of representing the dependence of dry deposition to vegetation parameters including drivers of stomatal resistance variation (change in CO_2, drought stress), especially when focusing on the impact of past or future changes of vegetation. Hardacre et al. (2015) recommend to provide more detailed diagnostics of O_3 dry deposition in next intermodel exercices to attribute the intermodal differences to methodology and/or representation of processes. The next generation of chemistry-transport models should therefore rely on online coupling with vegetation, with dry deposition schemes having a consistent and dynamic description of vegetation distribution and growth and related short-term (seasonal, annual variation) or long-term (past and future changes) evolutions. However, model intercomparisons focusing on each process considered in isolation with a proper shared methodology/set-up is crucial if one wants to progress in the understanding of the complex vegetation/atmospheric chemistry interactions. In particular the evolution of land cover maps should be considered as far as dry deposition is concerned in addition to emission changes in the next intermodel exercices aiming to project future atmospheric chemistry.

Acknowledgements

We warmly thank Oliver Wild for useful discussions on the model evaluation of dry deposition. Computer time was provided by the GENCI French supercomputing program. This research was supported by CNRS, via the INSU-LEFE French Program under the project BOTOX.

References

Andersson, C. and Engardt, M.: European ozone in a future climate: Importance of changes in dry deposition and isoprene emissions, J. Geophys. Res.-Atmos., 115, D02303, doi:10.1029/2008JD011690, 2010.

Dentener, F., et al. (2006), Nitrogen and sulfur deposition on regional and global scales: A multimodel evaluation, Global Biogeochem. Cycles, 20, GB4003, doi:10.1029/2005GB002672.

Dee, D. P., Uppala, S. M., Simmons, A. J., Berrisford, P., Poli, P., Kobayashi, S., Andrae, U., Balmaseda, M. A., Balsamo, G., Bauer, P., Bechtold, P., Beljaars, A. C. M., van de Berg, L., Bidlot, J., Bormann, N., Delsol, C., Dragani, R., Fuentes, M., Geer, A. J., Haimberger, L., Healy, S. B., Hersbach, H., Hólm, E. V., Isaksen, L., Kållberg, P., Köhler, M., Matricardi, M., McNally, A. P., Monge-Sanz, B. M., Morcrette, J.-J., Park, B.-K., Peubey, C., de Rosnay, P., Tavolato, C., Thépaut, J.-N. and Vitart, F. (2011), The ERA-Interim reanalysis: configuration and performance of the data assimilation system. Q.J.R. Meteorol. Soc., 137: 553–597. doi: 10.1002/qj.828.

Dufresne, J.-L., Foujols, M.-A., Denvil, S., Caubel, A., Marti, O., Aumont, O., Balkanski, Y., Bekki, S., Bellenger, H., Benshila, R., Bony, S., Bopp, L., Braconnot, P., Brockmann, P., Cadule, P., Cheruy, F., Codron, F., Cozic, A., Cugnet, D., de Noblet, N., Duvel, J.-P., Ethé, C., Fairhead, L., Fichefet, T., Flavoni, S., Friedlingstein, P., Grandpeix, J.-Y., Guez, L., Guilyardi, E., Hauglustaine, D., Hourdin, F., Idelkadi, A., Ghattas, J., Joussaume, S., Kageyama, M., Krinner, G., Labetoulle, S., Lahellec, A., Lefebvre, M.-P., Lefevre, F., Levy, C., Li, Z.X., Lloyd, J., Lott, F., Madec, G., Mancip, M., Marchand, M., Masson, S., Meurdesoif, Y., Mignot, J., Musat, I., Parouty, S., Polcher, J., Rio, C., Schulz, M., Swingedouw, D., Szopa, S., Talandier, C., Terray, P., Viovy, N., Vuichard, N., Climate change projections using the IPSL-CM5 Earth System Model: from CMIP3 to CMIP5, Clim. Dynamics, 40, doi: 10.1007/s00382-012-1636-1, 2013.

Folberth, G. A., Hauglustaine, D. A., Lathière, J., and Brocheton, F.: Interactive chemistry in the Laboratoire de Météorologie Dynamique general circulation model: model description and

impact analysis of biogenic hydrocarbons on tropospheric chemistry, Atmos. Chem. Phys., 6, 2273-2319, doi:10.5194/acp-6-2273-2006, 2006.

Fowler, D., Pilegaard, K., Sutton, M. A., Ambus, P., Raivonen, M., Duyzer, J., Simpson, D., Fagerli, H., Fuzzi, S., Schjoerring, J. K., Granier, C., Neftel, A., Isaksen, I. S. A., Laj, P., Maione, M., Monks, P. S., Burkhardt, J., Daemmgen, U., Neirynck, J., Personne, E., Wichink-Kruit, R., Butterbach-Bahl, K., Flechard, C., Tuovinen, J. P., Coyle, M., Gerosa, G., Loubet, B., Altimir, N., Gruenhage, L., Ammann, C., Cieslik, S., Paoletti, E., Mikkelsen, T. N., Ro-Poulsen, H., Cellier, P., Cape, J. N., Horvath, L., Loreto, F., Niinemets, U., Palmer, P. I., Rinne, J., Misztal, P., Nemitz, E., Nilsson, D., Pryor, S., Gallagher, M. W., Vesala, T., Skiba, U., Brueggemann, N., Zechmeister-Boltenstern, S., Williams, J., O'Dowd, C., Facchini, M. C., de Leeuw, G., Flossman, A., Chaumerliac, N., and Erisman, J.W.: Atmospheric composition change: Ecosystems-Atmosphere interactions, Atmos. Environ., 43, 5193–5267, doi:10.1016/j.atmosenv.2009.07.068, 2009.

Ganzeveld, L., Bouwman, L., Stehfest, E., Vuuren, D. P. V., Eickhout, B., and Lelieveld, J.: Impact of future land use and land cover changes on atmospheric chemistry-climate interactions, J. Geophys. Res., 115, D23301, doi:10.1029/2010JD014041, 2010.

Hardacre, C., Wild, O., and Emberson, L.: An evaluation of ozone dry deposition in global scale chemistry climate models, Atmos. Chem. Phys., 15, 6419-6436, doi:10.5194/acp-15-6419-2015, 2015.

Hauglustaine, D.A., Hourdin, F., Jourdain, L ., Filiberti, M.A., Walters, S., Lamarque, J.-F. and Holland, E.A.: Interactive chemistry in the Laboratoire de Meteorologie Dynamique general circulation model: Description and background tropospheric chemistry evaluation, J. Geophys. Res.-Atm., 109, D4, doi: D04314 10.1029/2003JD003957, 2004.

525 Hurtt, G. C., Chini, L. P., Frolking, S., Betts, R. A., Feddema, J., Fischer, G., Fisk, J. P., Hibbard,
526 K., Houghton, R. A., Janetos, A., Jones, C. D., Kindermann, G., Kinoshita, T., Goldewijk Kees
527 Klein Riahi, K. Shevliakova, E., Smith, S., Stehfest, E., Thomson, A., Thornton, P., van Vuuren,
528 D. P. and Wang, Y. P.: Harmonization of land-use scenarios for the period 1500-2100: 600 years
529 of global gridded annual land-use transitions, wood harvest, and resulting secondary lands,
530 Climatic Change, 109, 117-161, doi: 10.1007/s10584-011-0153-2, 2011.
531 Lamarque, J.-F., Bond, T. C., Eyring, V., Granier, C., Heil, A., Klimont, Z., Lee, D., Liousse, C.,
532 Mieville, A., Owen, B., Schultz, M. G., Shindell, D., Smith, S. J., Stehfest, E., Van Aardenne, J.,
533 Cooper, O. R., Kainuma, M., Mahowald, N., Mc-Connell, J. R., Naik, V., Riahi, K., and van
534 Vuuren, D. P.: Historical (1850–2000) gridded anthropogenic and biomass burning emissions of
535 reactive gases and aerosols: methodology and application, Atmos. Chem. Phys., 10, 7017–7039,
536 doi:10.5194/acp-10-7017-2010, 2010.
537 Lathière, J., Hauglustaine, D.A., De Noblet-Ducoudré, N., Krinner, G. and Folberth, G.A.: Past
538 and future changes in biogenic volatile organic compound emissions simulated with a global
539 dynamic vegetation model, Geophys. Res. Lett., 32, 20, doi: L20818 10.1029/2005GL024164,
540 2005.
541 Loveland, T. R., Reed, B. C., Brown, J. F., Ohlen, D. O., Zhu, Z., Yang, L., and Merchant, J. W.:
542 Development of a global land cover characteristics database and IGBP DISCover from 1 km
543 AVHRR data, Intern. J. Rem. Sens., 21(6–7), 1303–1330, 2000.
544 Moss, R.H., Edmonds, J.A., Hibbard, K.A., Manning, M.R., Rose, S.K., van Vuuren, D.P., Carter,
545 T.R., Emori, S., Kainuma, M., Kram, T., Meehl, G.A., Mitchell, J.F., Nakicenovic. N., Riahi, K.,
546 Smith, S.J., Stouffer, R.J., Thomson, A.M., Weyant, J.P. and Wilbanks, T.J.: The next generation
547 of scenarios for climate change research and assessment, Nature, 463, 7282, 747-756, doi:
548 10.1038/nature08823 FEB 11 2010, 2010.

549 Nowlan, C. R., Martin, R. V., Philip, S., Lamsal, L. N., Krotkov, N. A., Marais, E. A., Wang, S.
550 and Zhang, Q.: Global dry deposition of nitrogen dioxide and sulfur dioxide inferred from space-
551 based measurements, Global Biogeochem. Cy., 28, 1025–1043, doi:10.1002/2014GB004805,
552 2014.
553 Rayner, N.A., Parker, D.E., Horton, E.B., Folland, C.K., Alexander, L.V., Rowell, D.P., Kent,
554 E.C. and Kaplan, A.: Global analyses of sea surface temperature, sea ice, and night marine air
555 temperature since the late nineteenth century, J. of Geophys. Res.-Atm., 108, D14, 2156-2202,
556 doi: 10.1029/2002JD002670, 2003.
557 Sander, R.: Compilation of henry's law constants for inorganic and organic species of potential
558 importance in environmental chemistry (version 3), http://www.mpch-
559 mainz.mpg.de/sander/res/henry.html, 1999.
560 Stevenson, D.S., Dentener, F.J., Schultz, M.G., Ellingsen, K., van Noije, T.P.C., Wild, O., Zeng,
561 G., Amann, M., Atherton, C.S., Bell, N., Bergmann, D.J., Bey, I., Butler, T., Cofala, J., Collins,
562 W.J., Derwent, R.G., Doherty, R.M., Drevet, J., Eskes, H.J., Fiore, A.M., Gauss, M.,
563 Hauglustaine, D.A., Horowitz, L.W., Isaksen, I.S.A., Krol, M.C., Lamarque, J.F., Lawrence,
564 M.G., Montanaro, V., Muller, J.-F., Pitari, G., Prather, M.J., Pyle, J.A., Rast, S., Rodriguez, J.M.,
565 Sanderson, M.G., Savage, N.H., Shindell, D.T., Strahan, S.E., Sudo, K. and Szopa, S.:
566 Multimodel ensemble simulations of present-day and near-future tropospheric ozone, J. of
567 Geophys. Res.-Atm., 111, D8, doi: D08301 10.1029/2005JD006338, 2006.
568 Szopa, S., Balkanski, Y., Schulz, M., Bekki, S., Cugnet, D., Fortems-Cheiney, A., Turquety, S.,
569 Cozic, A., Deandreis, C., Hauglustaine, D., Idelkadi, A., Lathière, J., Lefèvre, F., Marchand, M.,
570 Vuolo, R., Yan, N. and Dufresne, J-L.: Aerosol and ozone changes as forcing for climate
571 evolution between 1850 and 2100, Climate Dynamics, 40, 9-10, 2223-2250, doi 10.1007/s00382-
572 012-1408-y, 2013.

573 Val Martin, M., Heald, C.L. and Arnold, S.R.: Coupling dry deposition to vegetation phenology
574 in the Community Earth System Model: Implications for the simulation of surface O_3, Geophys.
575 Res. Lett., 41, 2988–2996, doi:10.1002/2014GL059651, 2014.
576 van Vuuren, D.P., Edmonds, J., Kainuma, M., Riahi, K., Thomson, A., Hibbard, K., Hurtt, G.C.,
577 Kram, T., Krey, V., Lamarque, J.-F., Masui, T., Meinshausen, M., Nakicenovic, N., Smith, S.J.
578 and Rose, S.K.: The representative concentration pathways: an overview, Climatic Change, 109,
579 1-2, 5-31, doi: , 10.1007/s10584-011-0148-z, 2011.
580 Walcek, C.J., Brost, R.A., Chang, J.S., and Wesley, M.L., SO2, sulfate and HNO3 deposition
581 velocities computed using regional landuse and meteorological data, Atmospheric Environment,
582 20, 949-964, 1986.
583 Walmsley, J. L. and Wesely, M. L.: Modification of coded parametrizations of surface resistances
584 to gaseous dry deposition, Atmos. Environ., 30, 1181–1188, 1996.
585 Wesely, M.L.: Parameterization of surface resistances to gaseous dry deposition in regional-scale
586 numerical models, Atmos. Environ., 23, 6, 1293-1304, doi: 10.1016/0004-6981(89)90153-4,
587 1989.
588 Wesely, M.L. and Hicks, B.B.: A review of the current status of knowledge on dry deposition,
589 Atmos. Environ., 34, 2261 2282, doi: 10.1016/S1352-2310(99)00467-7, 2000.Zhang, L.M.,
590 Brook, J.R. and Vet, R.: On ozone dry deposition - with emphasis on non-stomatal uptake and
591 wet canopies, Atmos. Environ., 36, 30, 4787-4799, doi: 10.1016/S1352-2310(02)00567-8, 2002a.
592 Wu, S., Mickley, L. J., Kaplan, J. O., and Jacob, D. J.: Impacts of changes in land use and land
593 cover on atmospheric chemistry and air quality over the 21st century, Atmos. Chem. Phys., 12,
594 1597–1609, doi:10.5194/acp-12-1597-2012, 2012.

595 Zhang, L.M., Moran, M.D., Makar, P.A., Brook, J.R. and Gong, S.L.: Modelling gaseous dry
596 deposition in AURAMS: a unified regional air-quality modelling system, Atmos. Environ., 36, 3,
597 537-560, doi: 10.1016/S1352-2310(01)00447-2, 2002b.
598 Zhang, L., Brook, J. R., and Vet, R.: A revised parameterization for gaseous dry deposition in air-
599 quality models, Atmos. Chem. Phys., 3, 2067-2082, doi:10.5194/acp-3-2067-2003, 2003.
600

601 Table 1 : Simulations performed in our study with the LMDz-INCA chemistry-climate model : set-up description.

602

Run objectives	Land-cover map	Climate	Duration
CONTROL	Present-day 2000s	Winds and surface temperature nudged on ECMWF fields for 2007	1 year
IMPACT OF FUTURE LAND-USE CHANGES	2050 RCP 8.5	Winds and surface temperature nudged on ECMWF fields for 2007	1 year
	2050 RCP 4.5		
	2050 RCP 2.6		
IMPACT OF FUTURE CLIMATE	Present-day 2000s	2000-2010 fields (GCM mode)	10 years
		2045-2055 fields (GCM mode)	

603

604
605
606
607

608 Table 2 : Mean Effect on Annual Mean Surface Deposition Velocity (%) of climate and land cover changes of O_3 and
609 HNO_3 averaged over homogeneous regions (values > +-1.5% are highlighted)
610

	Ozone			Nitric Acid		
	Climate Change	RCP4.5 Land cover Change	Sum of Climate and Land cover Changes	Climate Change	RCP4.5 Land cover Change	Sum of Climate and Land cover Changes
GLOBAL	0.5	-0.7	-0.2	**2.2**	1.2	**3.4**
Eurasia	**2.1**	**-2.1**	0.0	**4.3**	**3.8**	**8.1**
USA	**1.5**	-1.3	0.2	**3.6**	**2.0**	**5.6**
Central America	-1.1	-1.4	**-2.6**	1.1	**1.7**	**2.8**
Tropical Southern America	**-2.3**	-1.2	**-3.5**	1.1	**2.6**	**3.7**
Tropical Africa	**-1.5**	-0.8	**-2.3**	0.4	0.9	1.3
South Africa	-1.4	-0.6	**-2.0**	-0.1	0.8	0.8
West Australia	-0.4	-0.1	-0.5	-0.4	0.0	-0.4
East Australia	-0.5	-0.6	-1.1	0.2	0.5	0.7
South America	0.4	-0.7	-0.4	0.3	**2.0**	**2.3**
Tropics	-1.1	-0.6	**-1.7**	0.6	1.0	**1.7**

611
612
613
614

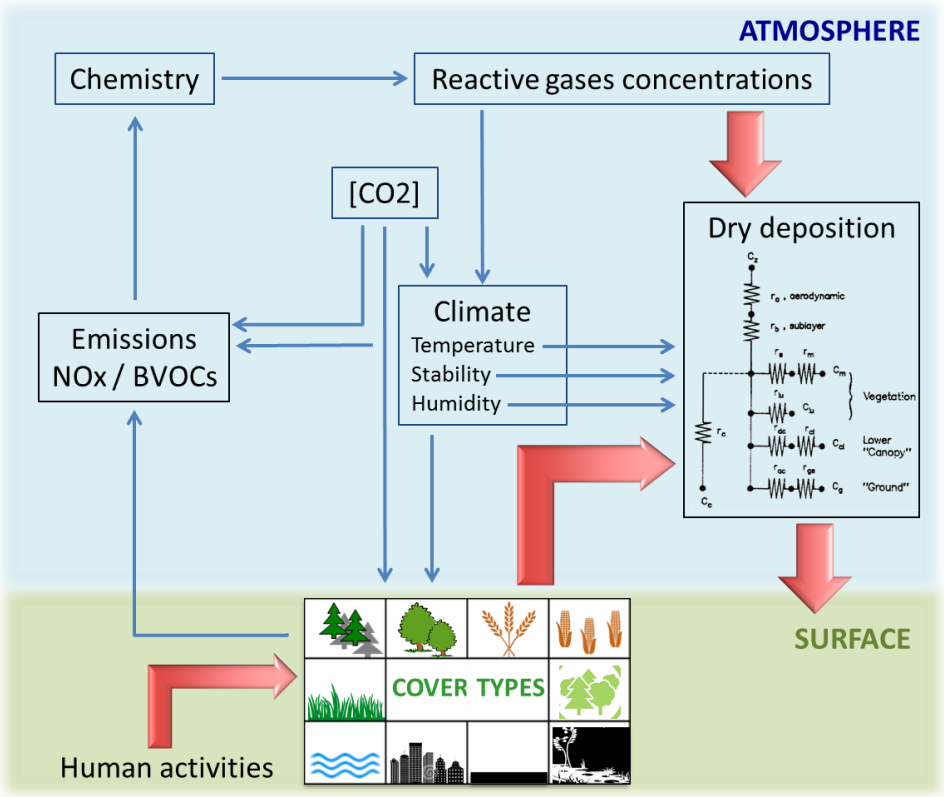

615

616 Figure 1: Interactions between vegetation and atmospheric chemistry potentially affected by land use changes. In this

617 work, only the red arrows are investigated.

618

619

620

621

622

623

624

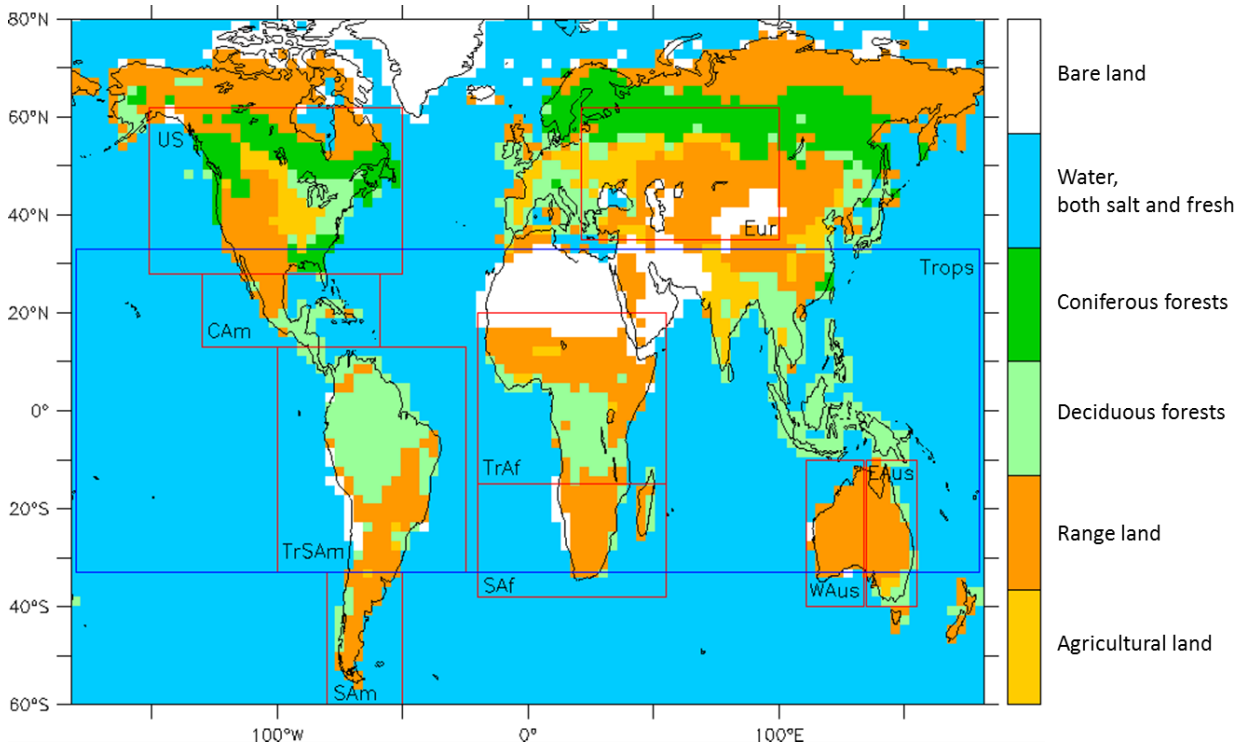

Figure 2: Surface categories considered in LMDz-INCA for dry deposition, represented as dominant coverage : agricultural land, range land, deciduous forest, coniferous forest, water, barren land, mostly desert. Regions discussed in this study are also illustrated: Eurasia, USA, Central America, Tropical Southern America, Southern America, Tropical Africa, Southern Africa, Western Australia, Eastern Australia and Tropical regions.

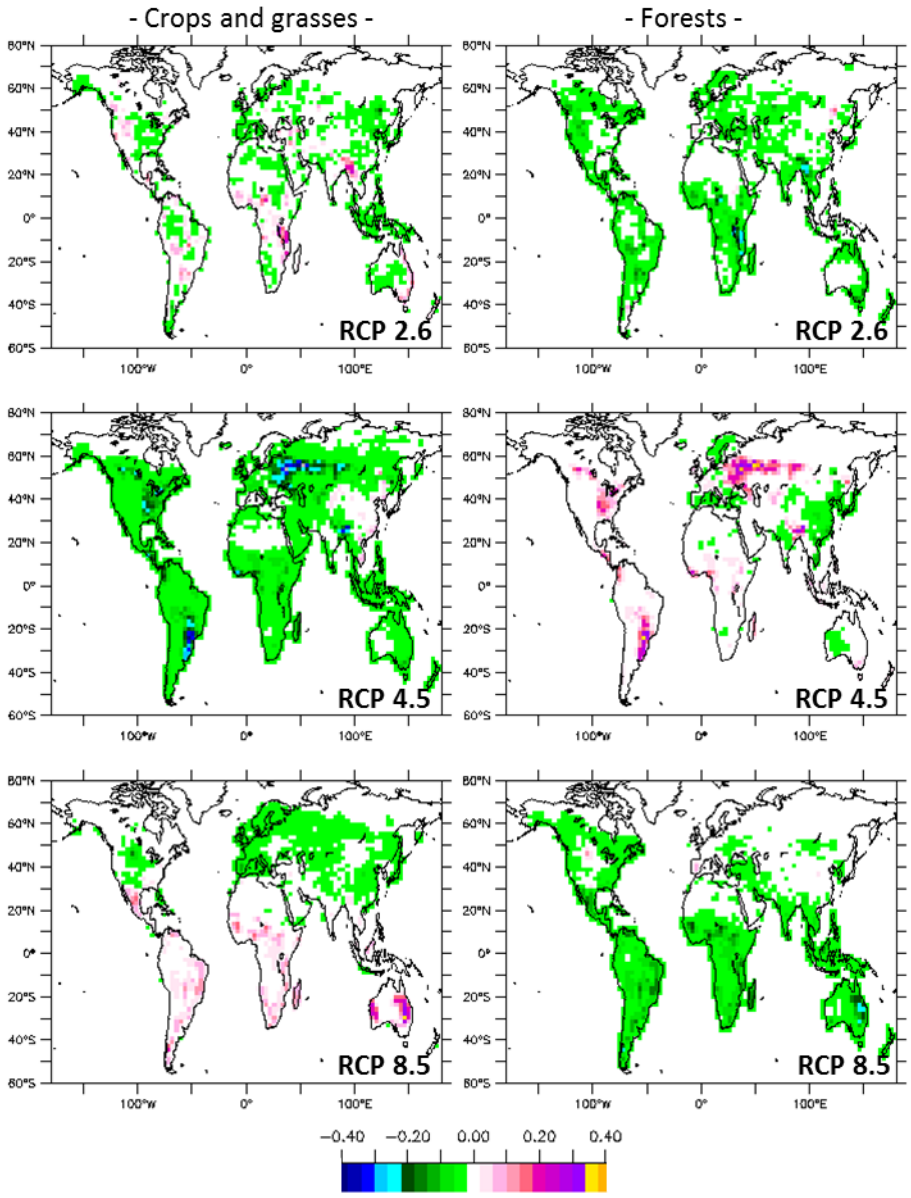

Figure 3: Vegetation fraction difference between 2050 and present-day for crops and grasses (left column), and forests (right column) according to the future RCP scenarios 2.6 (upper line), 4.5 (middle line) and 8.5 (lower line).

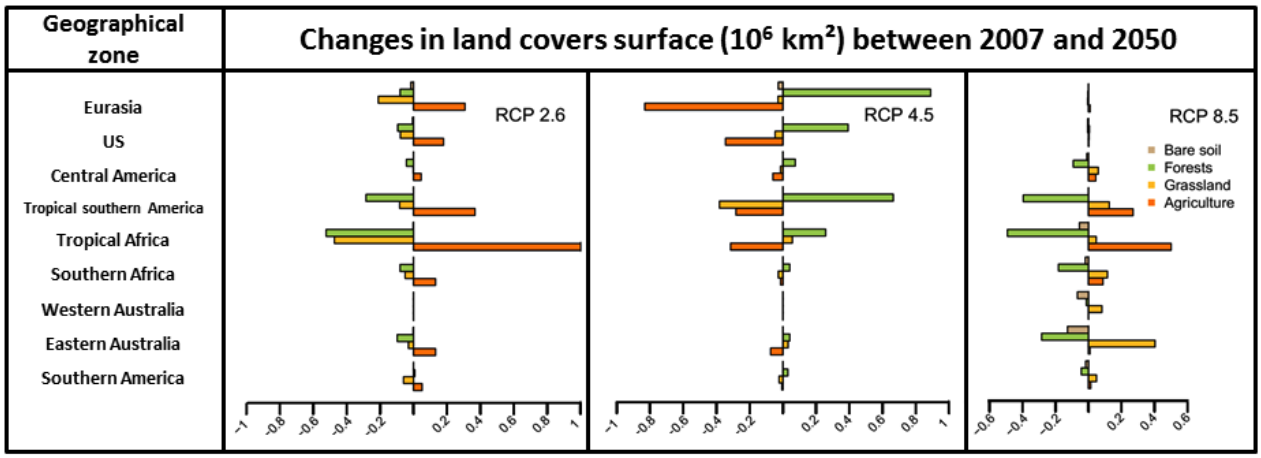

Figure 4: Changes between 2007 and 2050 in land-type surfaces (10^6 km²) for the nine regions as illustrated in figure 1, in the case of forests (green), crops (orange), grasses (yellow) and bare soil (brown).

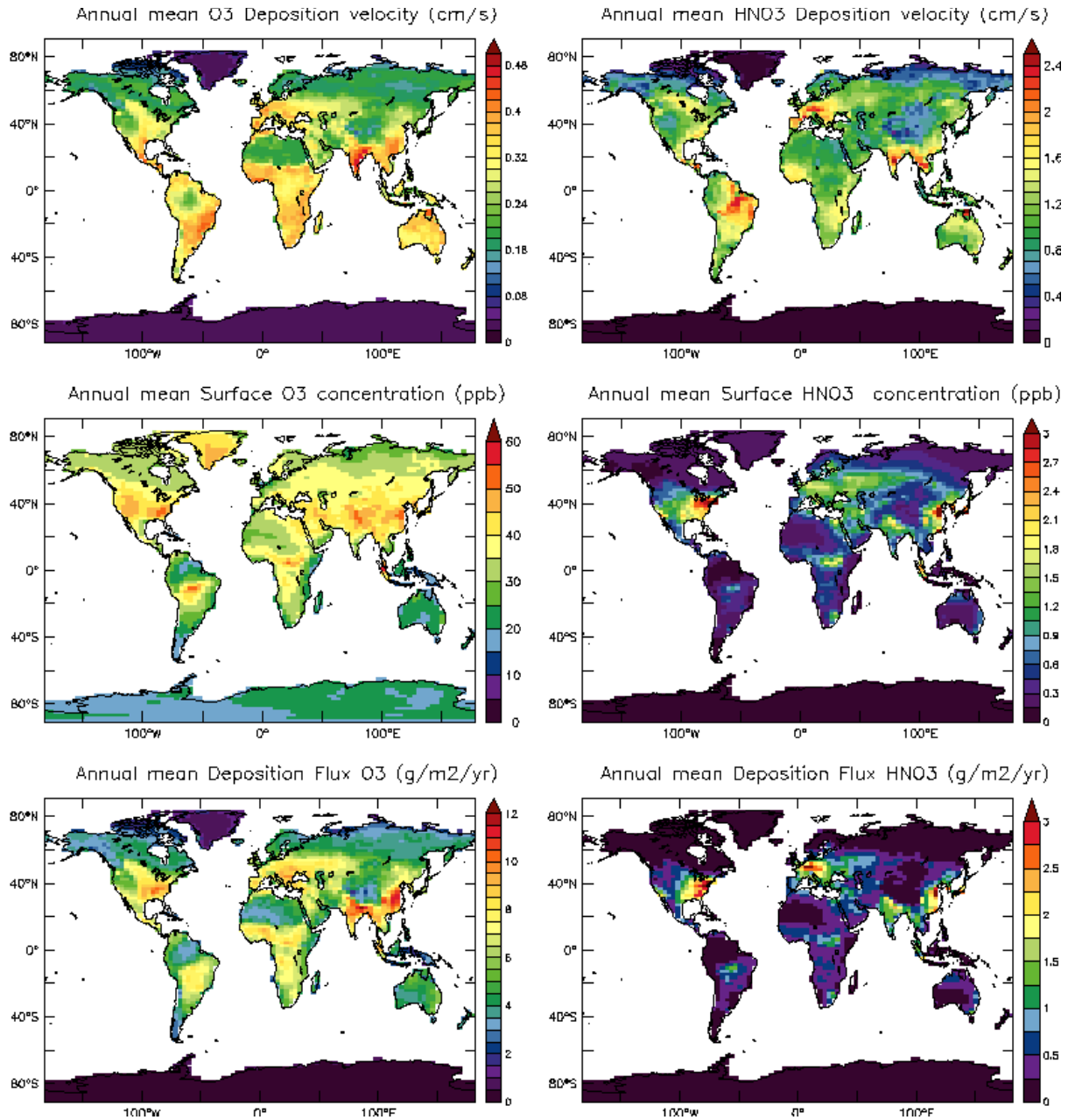

Figure 5: Annual average of surface dry deposition velocities (upper panel), surface concentrations (middle panel and deposition fluxes (lower panel) over continental surfaces (cm/s) for O_3 (left) and HNO_3 (right) for present-day as simulated by LMDz-INCA.

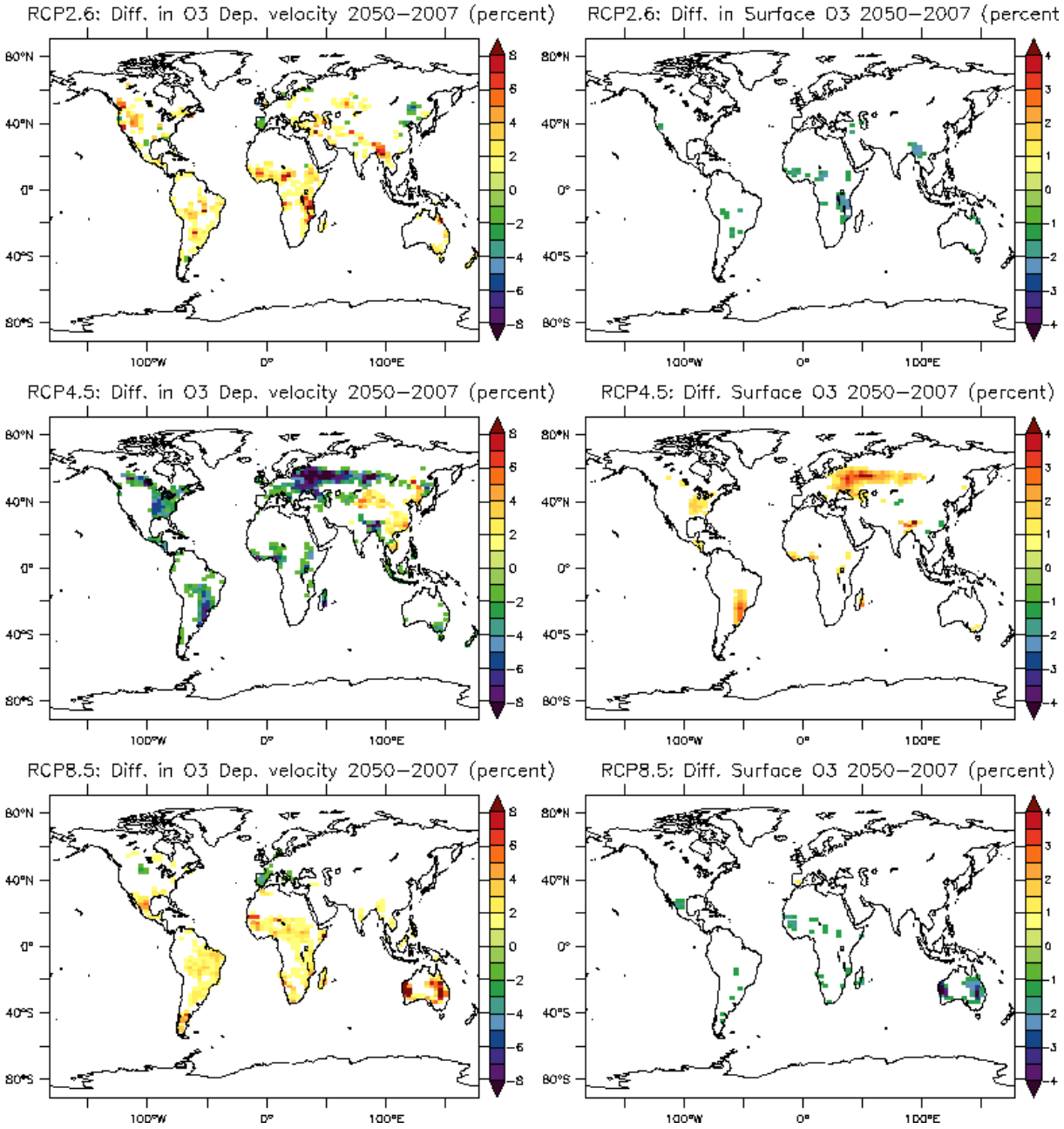

650

651 Figure 6: Annual mean changes (in relative value %) of surface dry deposition velocity for O_3 between present-day
652 and 2050 induced by the different LCC (Left) and related surface ozone concentrations (Right) for the three RCP
653 scenarios. Values in the [-1;+1]% interval are not shown

654

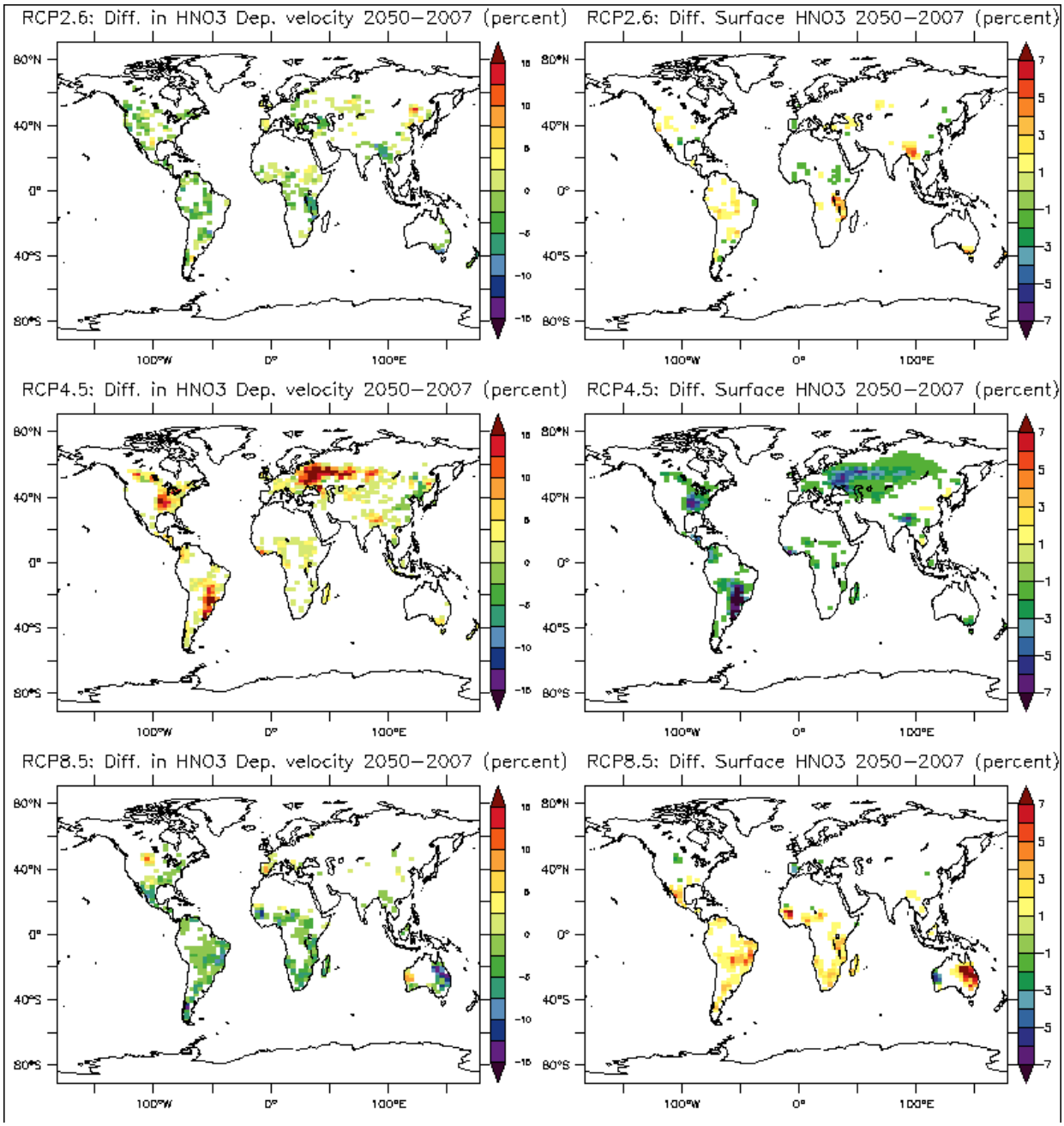

Figure 7: Same as Figure 6 for HNO_3.

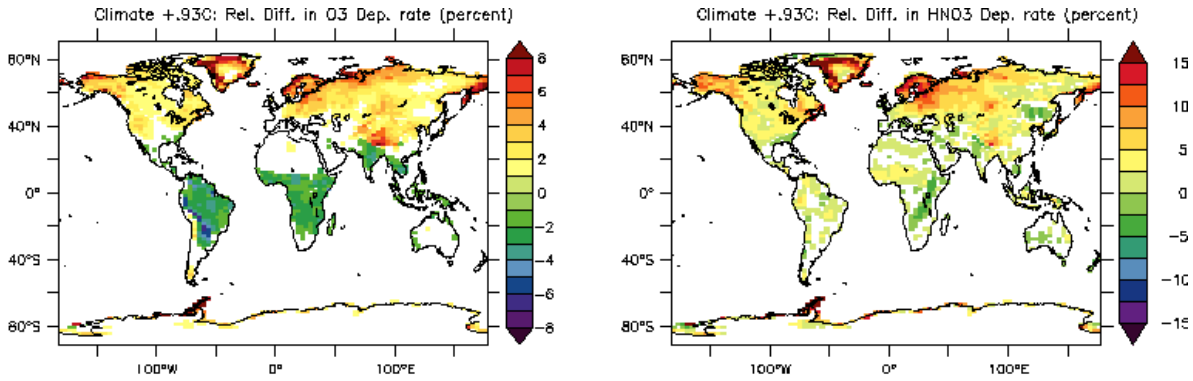

Figure 8: Future climate-induced impacts on surface dry deposition velocities (%) considering a 0.93°C increase of global temperature.